Optimal design of experiment

Oliwer Sliczniuk^{a,*}, Pekka Oinas^a

^{a}*Aalto University, School of Chemical Engineering, Espoo, 02150, Finland*

ARTICLE INFO

Keywords:
Supercritical extraction
Optimal design of experiment
Mathematical modelling

ABSTRACT

This study investigates the process of chamomile oil extraction from flowers. A parameter-distributed model consisting of a set of partial differential equations is used to describe the governing mass transfer phenomena in a solid-fluid environment under supercritical conditions using carbon dioxide as a solvent. The concept of quasi-one-dimensional flow is applied to reduce the number of spatial dimensions. The flow is assumed to be uniform across any cross-section, although the area available for the fluid phase can vary along the extractor. The physical properties of the solvent are estimated from the Peng-Robinson equation of state. The empirical correlations used in the model are based on the set of laboratory experiments performed under multiple constant operating conditions: $30 - 40°C$, $100 - 200$ bar, and $3.33 - 6.67 \cdot 10^{-5}$ kg/s. The model-based design of the experiments technique is applied in this work to improve the precision of the correlation parameters. The mass flow rate and the inlet temperature are used as decision variables to minimizing the volume of the confidence ellipsoid. As a result, the optimal control problem is numerically solved to obtain the controls, which maximises the Fisher information contained in the yield curve.

1. Introduction

This study investigates the extraction of essential oil from chamomile flowers (Matricaria chamomilla L.) via supercritical fluid extraction techniques and the modelling of this process. Chamomile is a medicinal herb widely cultivated in southern and eastern Europe in countries such as Germany, Hungary, France and Russia. It can be found outside Europe, for instance in Brazil as discussed by Singh et al. [1]. This plant is distinguished by its hollow, bright gold cones, housing disc or tubular florets and surrounded by about fifteen white ray or ligulate florets. Chamomile has been used for its medicinal benefits, serving as an anti-inflammatory, antioxidant, mild astringent, and healing remedy. Aqueous extract of chamomile is widely used to calm nerves and mitigate anxiety, hysteria, nightmares, insomnia and other sleep-related conditions, according to Srivastava [2]. Orav et al. [3] reported that oil yields from dried chamomile samples ranged from 0.7 to 6.7 mL/kg. The highest yields of essential oil, between 6.1 and 6.7 mL/kg, were derived from chamomile sourced from Latvia and Ukraine. In comparison, chamomile from Armenia exhibited a lower oil content of 0.7 mL/kg.

Evaluating the economic viability of the process is essential when choosing a suitable technology for essential oil extraction. Traditional methods, such as distillation and organic solvent extraction, are commonly employed but have drawbacks. Distillation, for example, involves high temperatures that can lead to the thermal degradation of heat-sensitive compounds. This limitation has led to the increased popularity of alternative techniques such as supercritical fluid extraction. Supercritical carbon dioxide is appealing thanks to its distinctive properties: it is inflammable, non-toxic and non-corrosive. Supercritical fluids can exhibit both gas- and liquid-like properties, allowing for adjustable dissolving power through changes in operating conditions.

The literature offers various mathematical models to describe the extraction of valuable compounds from biomass. Selecting a process model is case-to-case dependent and requires analysis of each model's specific assumptions about mass transfer and thermodynamic equilibrium.

The model proposed by Reverchon et al. [4] is called the hot ball model, as it is based on an analogy to heat transfer and describes an extraction process from solid particles. This model assumes that particles contain low quantities of solute and that solubility is not a limiting factor.

The Broken-and-Intact Cell model, proposed by Sovova [5], assumes that external surfaces of particles are mechanically disrupted, allowing the solvent access to the solute in the broken cells. In contrast, the solute in intact cells remains less accessible due to higher mass transfer resistance.

Reverchon [6] formulated a fluid-solid extraction model where the solute is treated as a single component, governed by internal mass transfer resistance and omitting the effects of external mass transfer, axial dispersion and variations in fluid density and flow rate throughout the bed.

This work builds upon the linear kinetic model suggested by Reverchon [6], deriving fundamental governing equations to develop a comprehensive model for the chamomile oil extraction process. This model aims for control-oriented simplicity, assuming a semi-continuous operation within a cylindrical vessel. The process involves a supercritical solvent being pumped through a fixed bed of finely chopped biomass to extract the solute, followed by separation of the solvent and solute in a flush drum to collect the extract. Parameters such as pressure (P), feed flow rate (F_{in}) and inlet temperature (T_{in}) are adjustable and measurable, while the outlet temperature (T_{out}) and the amount of product at the outlet can only be monitored. Figure 1 presents a simplified process flow diagram.

---

*Corresponding author

✉ oliwer.sliczniuk@aalto.fi (O. Sliczniuk)

ORCID(s): 0000-0003-2593-5956 (O. Sliczniuk); 0000-0002-0183-5558 (P. Oinas)
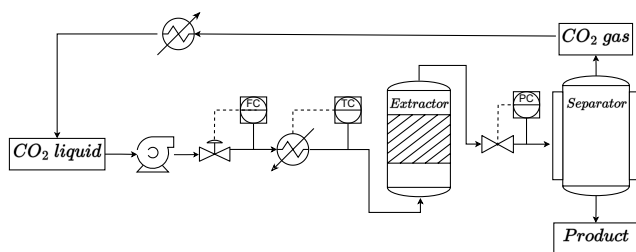
Figure 1: Process flow diagram

Design of Experiments (DoE) is a structured approach that examines how various elements influence a particular result. By evaluating multiple factors at once, DoE allows the uncovering of the impacts of each element and their combinations, yielding a comprehensive comprehension of the entire system. DoE begins with determining an experiment's objectives and selecting the study's process factors. DoE aims to obtain the maximum information from an experimental apparatus modelled by devising experiments that will yield the most informative data in a statistical sense for use in parameter estimation and model validation.

The first ideas of DoE were introduced by Fisher [7], who described the fundamental problem of experimental design as deciding what pattern of factors combination will best reveal the properties of the response, and this response is influenced by the factors. This type of DoE views an experiment as simply connecting inputs with outputs and is therefore called a "black-box experiment design". It aims to select the combinations of factor values that will provide the most information on the input-output relationship in the presence of variation. This type's main class of statistical design techniques is the so-called factorial method. These methods are created to measure the additive effects on a response for each input factor and investigate the effects of interactions between factors. Factorial methods are unsuitable for situations where constraints exist on the output or internal states. They must also be better suited for dynamic experiments, where inputs and outputs are complex time profiles. However, this group of methods is still widely used due to its simplicity.

The factorial methods can be used for parameter screening, giving main and interaction effects of the considered factors with fewer runs. Ramandi et al. [8] applied a full factorial design for screening the extraction parameters of fatty acids from *Borago officinalis L.* flowers by SFE technique before optimisation using central composition design. Four factors: temperature, pressure, modifier volume and static extraction time were considered independent variables for full factorial design. All these factors were studied at two levels.

Caldera et al. [9] optimised extraction parameters of SFE to extract antioxidant compounds from rosemary. 2^3 full factorial design was used to select important variables before optimisation of the selected factors by Box-Behnken design. Three factors, namely temperature, pressure and static extraction time, were studied in this experiment.

As opposed to the "black-box" statistical experiment design methods, another form of optimal design has been developed, which takes explicit advantage of some knowledge of the structure underlying the system, represented by a mathematical model, in particular in the form of differential and algebraic equations. What characterises the model-based experiment design approach is :

1. the explicit use of the model equations and current parameters to predict the "information content" of the next experiment

2. the application of an optimisation framework to the solution of the resulting numerical problem

After an initial dataset has been collected and fitted to a mathematical model, the model undergoes further analysis. Additional experiments may be designed and conducted to differentiate between competing models that passed the preliminary tests. Once inadequate models are rejected, the remaining model may undergo another round of experiment design to enhance the precision of its parameters. This paper focuses on the final step of the validation procedure, known as model-based Design of Experiments (DoE), aimed at improving parameter precision. To the authors' knowledge, the model-based design of dynamic experiments has not been applied to any case of supercritical extraction. The literature review below provides examples of this technique used in crystallization and pharmacology processes.

Chung et al. [10] applied model-based experimental design to a batch crystallization process with a cooling jacket. A dynamic programming formulation minimizes the volume of a confidence hyper-ellipsoid for the estimated nucleation and growth parameters over the supersaturation profile and the seed characteristics, namely, the crystal mass, mean size, and width of the seed distribution. As a result, the accuracy of the parameter estimates can be improved by identifying the optimal temperature profile.

Duarte et al. [11] investigated compartment models incorporating Michaelis-Menten elimination kinetics for pharmacological applications. The authors designed both static and dynamic experiments for 2- and 3-compartment models using D-optimality criteria. The dynamic experiments for both models involved determining the initial concentration in the first compartment and optimizing the profile of the mass flow rate of the drug entering this compartment.

2. Materials and methods

2.1. Governing equations

Following the work of Anderson [12], the governing equations for a quasi-one-dimensional flow were derived. A quasi-one-dimensional flow refers to a fluid flow scenario assuming that the flow properties are uniformly distributed across any cross-section. This simplification is typically applied when the flow channel's cross-sectional area changes, such as through irregular shapes or partial filling of an extractor. According to this assumption, velocity and other flow properties change solely in the flow direction.

As discussed by Anderson [13], all flows are compressible, but some of them can be treated as incompressible when the Mach number is smaller than 0.3. This assumption leads to the incompressible condition: $\nabla \cdot u = 0$, which is valid for constant density (strict incompressible) or varying density flow. The assumption allows for removing acoustic waves and large perturbations in density and/or temperature. In the 1-D case, the incompressibility condition becomes $\frac{du}{dz} = 0$, so the fluid velocity is constant.

The set of quasi-one-dimensional governing equations in Cartesian coordinates is described by Equations 1 - 3:

$$\frac{\partial \left(\rho_f A_f\right)}{\partial t} + \frac{\partial \left(\rho_f A_f v\right)}{\partial z} = 0 \tag{1}$$

$$\frac{\partial \left(\rho_f v A_f\right)}{\partial t} + \frac{\partial \left(\rho_f A_f v^2\right)}{\partial z} = -A_f \frac{\partial P}{\partial z} \tag{2}$$

$$\frac{\partial \left(\rho_f e A_f\right)}{\partial t} + \frac{\partial \left(\rho_f A_f v e\right)}{\partial z} = -P \frac{\left(A_f v\right)}{\partial z} + \frac{\partial}{\partial z}\left(k \frac{\partial T}{\partial z}\right) \tag{3}$$

where ρ_f is the density of the fluid, A_f is the function which describes a change in the cross-section, v is the velocity, P is the total pressure, e is the internal energy of the fluid, t is time and z is the spatial direction.

2.2. Extraction model
2.2.1. Continuity equation
The previously derived quasi-one-dimensional continuity equation (Equation 1) is redefined by incorporating the function $A_f = A\phi$. This modification distinguishes constant and varying terms, where the varying term accounts for changes in the cross-sectional area available for the fluid. Equation 4 shows the modified continuity equation:

$$\frac{\partial(\rho_f \phi)}{\partial t} + \frac{\partial(\rho_f v A \phi)}{\partial z} = 0 \tag{4}$$

where A is the total cross-section of the extractor and ϕ describes porosity along the extractor.

Assuming that the mass flow rate is constant in time, the temporal derivative becomes the mass flux F, and the spatial derivative can be integrated along z as

$$\int \frac{\partial(\rho_f v A \phi)}{\partial z} dz = F \rightarrow F = \rho_f v A \phi \tag{5}$$

To simplify the system dynamics, it is assumed that F is a control variable and affects the whole system instantaneously (due to $\nabla \cdot u = 0$), which allows finding the velocity profile that satisfies mass continuity based on F, ϕ and ρ_f:

$$v = \frac{F}{\rho_f A \phi} \tag{6}$$

Similarly, superficial velocity may be introduced:

$$u = v\phi = \frac{F}{\rho_f A} \tag{7}$$

The fluid density ρ_f can be obtained from the Peng-Robinson equation of state if the temperature and thermodynamic pressure are known along z. Variation in fluid density may occur due to pressure or inlet temperature changes. In a non-isothermal case, in Equations 6 and 7 ρ_f is considered the average fluid density along the extraction column.

2.2.2. Mass balance for the fluid phase
Equation 8 describes the movement of the solute in the system, which is constrained to the axial direction due to the quasi-one-dimensional assumption. Given that the solute concentration in the solvent is negligible, the fluid phase is described as pseudo-homogeneous, with properties identical to those of the solvent itself. It is also assumed that the thermodynamic pressure remains constant throughout the device. The analysis further simplifies the flow dynamics by disregarding the boundary layer near the extractor's inner wall. This leads to a uniform velocity profile across any cross-section perpendicular to the axial direction. Thus, the mass balance equation includes convection, diffusion and kinetic terms representing the fluid phase behaviour:

$$\frac{\partial c_f}{\partial t} + \frac{1}{\phi}\frac{\partial \left(c_f u\right)}{\partial z} = \frac{1-\phi}{\phi} r_e + \frac{1}{\phi}\frac{\partial}{\partial z}\left(D_e^M \frac{\partial c_f}{\partial z}\right) \tag{8}$$

where c_f represents the solute concentration in the fluid phase, r_e is the mass transfer kinetic term and D_e^M is the axial diffusion coefficient.

### 2.2.3. Mass balance for the solid phase
As given by Equation 9, the solid phase is considered stationary, without convection and diffusion terms in the mass balance equation. Therefore, the only significant term in this equation is the kinetic term of Equation 10, which connects the solid and fluid phases. For simplicity, the extract is represented by a single pseudo-component:

$$\frac{\partial c_s}{\partial t} = \underbrace{r_e}_{\text{Kinetics}} \tag{9}$$

2.2.4. Kinetic term
As the solvent flows through the bed, CO_2 molecules diffuse into the pores and adsorb on the particle surface to form an external fluid film around the solid particles due to the solvent-solid matrix interactions. The dissolved solute diffuses from the particle's core through the solid-fluid interface, the pore and the film into the bulk. Figure 2 shows the mass transfer mechanism, where the mean solute concentration in the solid phase is denoted as c_s, and the equilibrium concentrations at the solid-fluid interface are denoted as c_s^* and c_p^* for the solid and fluid phases, respectively. The concentration of the solutes in the fluid phase in the centre of the pore is denoted as c_p. As the solute diffuses through the pore, its concentration changes and reaches c_{pf} at the pore opening. Then, the solute diffuses through the film around the particle and reaches bulk concentration c_f. The two-film theory describes the solid-fluid interface inside the pore. The overall mass transfer coefficient can be determined from the relationship between the solute concentration in one phase and its equilibrium concentration.

Bulley et al. [14] suggest a process where the driving force for extraction is given by the difference between the concentration of the solute in the bulk, c_f, and in the centre of the pore, c_p^*. The concentration c_p^* is in equilibrium with c_s according to the equilibrium relationship. The rate of extraction is thus $r_e\left(c_f - c_p^*(c_s)\right)$. In contrast, Reverchon
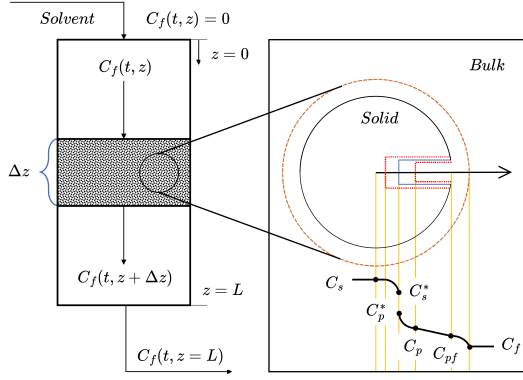
Figure 2: Mass transfer mechanism.

[6] proposes a driving force given by the difference between c_s and c_p^*. Concentration c_p^* is determined by the equilibrium relationship with c_f and the extraction rate given by Equation 10:

$$r_e = \frac{D_i}{\mu l^2} \left(c_s - c_p^* \right) \tag{10}$$

where μ is sphericity, l a characteristic dimension of particles that can be defined as $l = r/3$, r is the mean particle radius, ρ_s is the solid density, D_i corresponds to the overall diffusion coefficient and c_P^* is the concentration at the solid-fluid interface (which according to the internal resistance model is supposed to be at equilibrium with the fluid phase).

According to Bulley et al. [14], a linear equilibrium relationship (Equation 11) can be used to find the equilibrium concentration of the solute in the fluid phase c_f^* based on the concentration of the solute in the solid phase c_s:

$$c_f^* = k_p c_s \tag{11}$$

The volumetric partition coefficient k_p acts as an equilibrium constant between the solute concentration in one phase and the corresponding equilibrium concentration at the solid-fluid interphase. According to Spiro and Kandiah [15], k_p can be expressed through the mass partition coefficient k_m:

$$k_m = \frac{k_p \rho_s}{\rho_f} \tag{12}$$

According to Reverchon [6], the kinetic term becomes

$$r_e = -\frac{D_i}{\mu l^2} \left(c_s - \frac{\rho_s c_f}{k_m \rho_f} \right) \tag{13}$$

2.2.5. Uneven solute's distribution in the solid phase

Following the idea of the Broken-and-Intact Cell (BIC) model (Sovova [16]), the internal diffusion coefficient D_i is considered to be a product of the reference value of D_i^R and the exponential decay function γ, as given by Equation 14:

$$D_i = D_i^R \gamma(c_s) = D_i^R \exp \left(\Upsilon \left(1 - \frac{c_s}{c_{s0}} \right) \right) \tag{14}$$

where Υ describes the curvature of the decay function. Equation 15 describes the final form of the kinetic term:

$$r_e = -\frac{D_i^R \gamma}{\mu l^2} \left(c_s - \frac{\rho_s c_f}{k_m \rho_f} \right) \tag{15}$$

The γ function limits the solute's availability in the solid phase. Similarly to the BIC model, the solute is assumed to be contained in the cells, some of which are open because the cell walls were broken by grinding, with the rest remaining intact. The diffusion of the solute from a particle's core takes more time than the diffusion of the solute close to the outer surface. The same idea can be represented by the decaying internal diffusion coefficient, where the decreasing term is a function of the solute concentration in the solid.

Alternatively, the decay function γ can be interpreted by referring to the Shrinking Core model presented by Goto et al. [17], where the particle radius changes as the amount of solute in the solid phase decreases. As the particle size decreases due to dissolution, the diffusion path increases, which makes the diffusion slower and reduces the value of the diffusion coefficient. This analogy can be applied to Equation 14 to justify the application of a varying diffusion coefficient.

2.2.6. Empirical correlations

The empirical correlations for D_i and Υ were derived by article 1 and validated for temperatures between $30 - 40°C$, pressures between $100 - 200$ bar, and mass flow rates between $3.33 - 6.67 \cdot 10^{-5}$ kg/s. Figures 3 and 4 show the results of multiple linear regression applied to solutions of parameter estimation and selected independent variables.
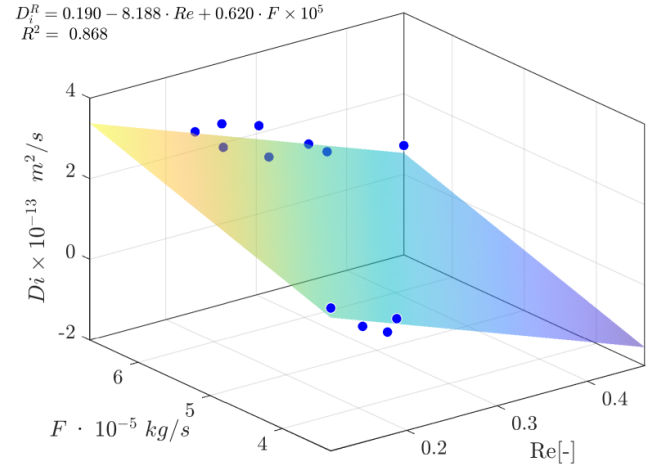
Figure 3: Multiple linear regression $D_i^R = f(Re, F)$

2.2.7. Heat balance

The heat balance equation describe the evolution of the enthalpy in the system and it is given by Equation 16
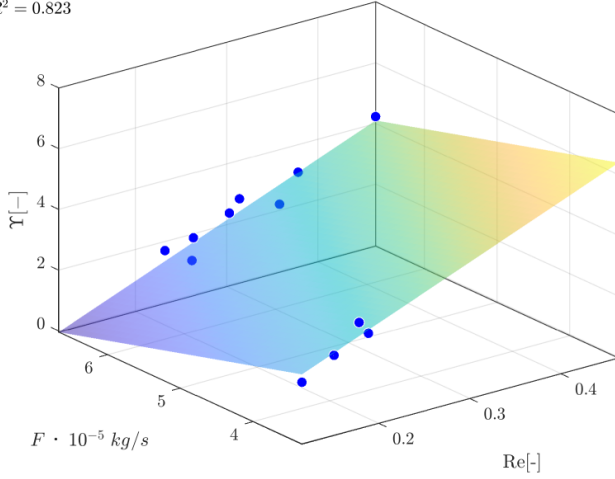
$$\frac{\partial \left(\rho_f h A_f \right)}{\partial t} = -\frac{\partial \left(\rho_f h A_f v \right)}{\partial z} + \frac{\partial \left(P A_f \right)}{\partial t} + \frac{\partial}{\partial z} \left(k \frac{\partial T}{\partial z} \right) \tag{16}$$

If the value of enthalpy h is known from the time evolution of the energy equation, and pressure P is known from measurement, then the temperature T can be reconstructed based on the departure function. The departure function is

$$\Upsilon = 3.158 + 11.922 \cdot Re - 0.686 \cdot F \times 10^5$$
$$R^2 = 0.823$$

Figure 4: Multiple linear regression $\Upsilon = f(Re, F)$

a mathematical function that characterizes the deviation of a thermodynamic property (enthalpy, entropy, and internal energy) of a real substance from that of an ideal gas at the same temperature and pressure. As presented by Gmehling et al. [18], for the Peng-Robinson equation of state, the enthalpy departure function is defined by Equation 17.

$$h - h^{id} = RT \left[T_r(Z-1) - 2.078(1+\kappa)\sqrt{\alpha(T)} \ln\left(\frac{Z + \left(1+\sqrt{2}\right)B}{Z + \left(1-\sqrt{2}\right)B}\right) \right] \quad (17)$$

where α is defined as $\left(1 + \kappa\left(1 - \sqrt{T_r}\right)\right)^2$, T_r is the reduced temperature, P_r is the reduced pressure, Z is the compressibility factor, κ is a quadratic function of the acentric factor and B is calculated as $0.07780\frac{P_r}{T_r}$.

Equation 17 requires an reference sate, which is assumed to be $T_{ref} = 298.15$ K and $P_{ref} = 1.01325$ bar.

A root-finder can be used to find a value of temperature, which minimizes the difference between the value of enthalpy coming from the heat balance and the departure functions. The root fining procedure to repeated at every time step to find a temperature profile along spatial direction z.

$$\min_{T} \left(\underbrace{h(t,x)}_{\text{Heat balance}} - \underbrace{h\left(T, P, \rho_f(T, P)\right)}_{\text{Departure function}} \right)^2 \quad (18)$$

2.2.8. Pressure term

As explained in Chapters 2.1, at Low-Mach number conditions, the thermodynamic pressure is nearly constant in space due to the small pressure wave propagation that occurs at the speed of sound. Under such conditions, the term $\partial P/\partial t$ can be approximated by a difference equation, which describes the pressure change in the whole system. The pressure P in the system is considered a state variable, while the pressure in the new time-step P_{in} is considered a control variable.

$$\frac{\partial P}{\partial t} \approx \frac{P_{in} - P}{\Delta t} \quad (19)$$

Such a simplified equation allows for instantaneous pressure change in the system but does not consider a gradual pressure build-up and the effects of pressure losses. In a real system, the dynamics of pressure change would depend on a pump and a back-pressure regulator.

2.2.9. Extraction yield

The process yield is calculated according to Equation 20 as presented by Sovova et al. [19]. The measurement equation evaluates the solute's mass at the extraction unit outlet and sums it up. The integral form of the measurement (Equation 20) can be transformed into the differential form (Equation 21) and augmented with the process model.

$$y = \int_{t_0}^{t_f} \frac{F}{\rho_f} c_f \Big|_{z=L} dt \quad (20)$$

$$\frac{dy}{dt} = \frac{F}{\rho_f} c_f \Big|_{z=L} \quad (21)$$

2.2.10. Initial and boundary conditions

It is assumed that the solvent is free of solute at the beginning of the process $c_{f0} = 0$, that all the solid particles have the same initial solute content c_{s0}, and that the system is isothermal, hence the initial state is h_0. The fluid at the inlet is considered not to contain any solute. The initial and boundary conditions are defined as follows:

$$c_f(t=0, z) = 0 \qquad c_s(t=0, z) = c_{s0} \qquad h(t=0, z) = h_0$$

$$c_f(t, z=0) = 0 \qquad h(t, z=0) = h_{in} \qquad \frac{\partial c_f(t, z=L)}{\partial x} = 0$$

$$\frac{\partial h(t, z=L)}{\partial x} = 0 \qquad c_s(t, z=\{0, L\}) = 0 \qquad y(0) = 0 \quad P(0) = P_0$$

2.2.11. Discretization methods

The method of lines is used to transform the process model equations into a set of ODEs denoted as $G(x; \Theta)$. The backward finite difference is used to approximate the first-order derivative, while the central difference scheme approximates the second-order derivative z direction. The length of the fixed bed is divided into N_z, i.e. equally distributed points in the z direction. The state-space model after discretization is denoted as x and defined as follows:

$$\dot{x} = \frac{dx}{dt} = \begin{bmatrix} \frac{dc_{f,1}}{dt} \\ \vdots \\ \frac{dc_{f,N_z}}{dt} \\ \frac{dc_{s,1}}{dt} \\ \vdots \\ \frac{dc_{s,N_z}}{dt} \\ \frac{dh_1}{dt} \\ \vdots \\ \frac{dh_{N_z}}{dt} \\ \frac{dP}{dt} \\ \frac{dy}{dt} \end{bmatrix} = \underbrace{\begin{bmatrix} G_1\left(c_f,c_s,h;\Theta\right) \\ \vdots \\ G_{N_z}\left(c_f,c_s,h;\Theta\right) \\ G_{N_z+1}\left(c_f,c_s,h;\Theta\right) \\ \vdots \\ G_{2N_z}\left(c_f,c_s,h;\Theta\right) \\ G_{2N_z+1}\left(c_f,c_s,h;\Theta\right) \\ \vdots \\ G_{3N_z}\left(c_f,c_s,h;\Theta\right) \\ G_{3N_z+1}\left(c_f,c_s,h;\Theta\right) \\ G_{3N_z+2}\left(c_f,c_s,h;\Theta\right) \end{bmatrix}}_{G(x;\Theta)}$$

where $x \in \mathbb{R}^{N_x = 3N_z+2}$ and $\Theta \in \mathbb{R}^{N_\Theta = N_\theta + N_u}$, N_θ is the number of parameters, N_u is the number of control variables.

For a derivative to be conservative, it must form a telescoping series. In other words, only the boundary terms should remain after adding all terms coming from the discretization over a grid, and the artificial interior points should be cancelled out. Discretization is applied to the conservative form of the model to ensure mass conservation.

2.3. Optimal design of experiment
2.3.1. Maximum likelihood

Following the work of Walter and Pronzato [20], the vector $\hat{\Theta}_{ml}$ will be a maximum-likelihood estimate if it maximizes the cost function:

$$j_{ml}(\Theta) = \pi_y(Y|\Theta) \tag{22}$$

If Θ were fixed, $\pi_y(Y|\Theta)$ would be the probability density of the random vector Y generated by a model with parameters Θ and observations Y. Considered as a function of Θ, $\pi_y(Y|\Theta)$ is then called the likelihood of Y. The maximum-likelihood method looks for the parameter vector Θ value that gives the observed data the highest likelihood. In practice, it is often easier to look for $\hat{\Theta}_{ml}$ by maximizing the log-likelihood function, yielding the same estimate since the logarithm function is monotonically increasing.

$$j_{ml}(\Theta) = \ln(\pi_y(Y|\Theta)) \tag{23}$$

Assume that the observed outputs satisfy

$$Y(t_i) = y(t_i, \Theta^*) + \epsilon_i, \qquad i = 1, ..., n_t \tag{24}$$

where the vector $y(t_i, \Theta^*)$ is the output of a deterministic model, Θ^* is the true value of the parameter vector, and the error ϵ_i belongs to a sequence of independent random variables with probability density $\pi_\epsilon(\epsilon_i)$. Since the ϵ_i are independent

$$\pi_\epsilon(\epsilon_1, \epsilon_2, ..., \epsilon_{n_t}) = \prod_{i=1}^{n_t} \pi_{\epsilon_i}(\epsilon_i) \tag{25}$$

Consider the output error

$$e^y(t_i, \Theta) = Y(t_i) - y(t_i, \Theta) \tag{26}$$

For the true value of the parameters, it satisfies $e^y(t_i, \Theta^*) = \epsilon_i$. and, since y is deterministic, $\pi_{y_i}(Y(t_i)|\Theta) = \pi_{\epsilon_i}(e^y(t_i), \Theta)$. The likelihood of the n_t observations can be written as

$$\pi_y(Y|\Theta) = \prod_{i=1}^{n_t} \pi_{\epsilon_i}(e^y(t_i, \Theta)) = \prod_{i=1}^{n_t} \pi_{\epsilon_i}(Y(t_i) - y(t_i, \Theta)) \tag{27}$$

If the noise is assumed to follow the normal distribution with the standard deviation σ, which is known from the parameter estimation:

$$\pi_y(Y|\Theta) = \prod_{i=1}^{n_t} \frac{1}{\sqrt{2\pi\sigma_{t_i}^2}} \exp\left[-\frac{1}{2}\left(\frac{Y(t_i) - y(t_i, \Theta)}{\sigma_{t_i}}\right)^2\right] \tag{28}$$

The associated log-likelihood can be written as

$$\ln(\pi_y(Y|\Theta)) = (\text{term independent of } \Theta) - \frac{1}{2}\sum_{i=1}^{n_t}\left(\frac{Y(t_i) - y(t_i, \Theta)}{\sigma_{t_i}}\right)^2 \tag{29}$$

Its gradient is thus

$$\frac{\partial}{\partial\Theta}\ln(\pi_y(Y|\Theta)) = \sum_{i=1}^{n_t}\left[\left(\frac{Y(t_i) - y(t_i, \Theta)}{\sigma_{t_i}^2}\right)\frac{\partial y(t_i, \Theta)}{\partial\Theta}\right] \tag{30}$$

2.3.2. Fisher information

The Fisher information is a way of measuring the amount of information that an observable random variable carries about an unknown parameter of a distribution that models the random variable. The Fisher information is related to the second derivative (or the curvature) of the log-likelihood function with respect to the parameter. This relationship provides a measure of how "sensitive" the likelihood is to changes in the parameter value. The Fisher information matrix $\mathcal{F}$ can be calculated as follow.

$$\mathcal{F}(\Theta) = -\underset{Y|\Theta}{\mathbb{E}}\left[\frac{\partial^2 \ln(\pi_y(Y|\Theta))}{\partial\Theta\partial\Theta^\top}\right] = \underset{Y|\Theta}{\mathbb{E}}\left[\frac{\partial \ln(\pi_y(Y|\Theta))}{\partial\Theta}\frac{\partial \ln(\pi_y(Y|\Theta))}{\partial\Theta^\top}\right]$$

$$= \underset{Y|\Theta}{\mathbb{E}}\left[\sum_{k=1}^{n_t}\left(\frac{Y(t_k) - y(t_k, \Theta)}{\sigma_{t_k}^2}\frac{\partial y(t_k, \Theta)}{\partial\Theta}\right) \times \sum_{i=1}^{n_t}\left(\frac{Y(t_i) - y(t_i, \Theta)}{\sigma_{t_i}^2}\frac{\partial y(t_i, \Theta)}{\partial\Theta^\top}\right)\right]$$

$$= \underset{Y|\Theta}{\mathbb{E}}\left[\sum_{k=1}^{n_t}\sum_{i=1}^{n_t}\left[\left(\frac{Y(t_k) - y(t_k, \Theta)}{\sigma_{t_k}^2}\frac{\partial y(t_k, \Theta)}{\partial\Theta}\right) \times \left(\frac{Y(t_i) - y(t_i, \Theta)}{\sigma_{t_i}^2}\frac{\partial y(t_i, \Theta)}{\partial\Theta^\top}\right)\right]\right]$$

$$= \sum_{k=1}^{n_t}\sum_{i=1}^{n_t}\underset{Y|\Theta}{\mathbb{E}}\left[\left(\frac{Y(t_k) - y(t_k, \Theta)}{\sigma_{t_k}^2}\frac{\partial y(t_k, \Theta)}{\partial\Theta}\right) \times \left(\frac{Y(t_i) - y(t_i, \Theta)}{\sigma_{t_i}^2}\frac{\partial y(t_i, \Theta)}{\partial\Theta^\top}\right)\right]$$

$$= \sum_{k=1}^{n_t}\sum_{i=1}^{n_t}\frac{1}{\sigma_{t_k}^2}\frac{\partial y(t_k, \Theta)}{\partial\Theta}\frac{1}{\sigma_{t_i}^2}\frac{\partial y(t_i, \Theta)}{\partial\Theta^\top}\underset{Y|\Theta}{\mathbb{E}}\left[(Y(t_k) - y(t_k, \Theta)) \times (Y(t_i) - y(t_i, \Theta))\right]$$

Considering the mismatch between the dataset and the model output, the Equation 26 can be used to redefine the expectation $\mathbb{E}_{Y|\Theta}$ as $\mathbb{E}_{Y|\Theta}\left[(Y(t_i) - y(t_i, \Theta))(Y(t_k) - y(t_k, \Theta))\right] = \mathbb{E}_{Y|\Theta}\left[\epsilon_i \epsilon_k\right]$. For $i = k$, the expectation of ϵ_i is the variance of the noise $\sigma_{t_i}^2$. Analogously, the expectation becomes 0 if $i \neq k$ because the measurement noises are independent at different times.

$$\underset{Y|\Theta}{\mathbb{E}}\left[(Y(t_i) - y(t_k, \Theta))(Y(t_k) - y(t_i, \Theta))\right] = \sigma_{t_i}^2 \delta_{ik} \tag{31}$$

where δ_{ik} represents the Kronecker delta. Given the property of the Kronecker delta, the double summation in the Fisher Information matrix reduces to a single summation:

$$\mathcal{F}(\Theta) = \sum_{i=1}^{n_t} \left(\frac{1}{\sigma_{t_i}^2} \frac{\partial y(t_i, \Theta)}{\partial \Theta} \frac{\partial y(t_i, \Theta)}{\partial \Theta^\top} \right) \tag{32}$$

If every experiment at time t_i is independent and characterized by its own σ_{t_i}, then the Fisher information matrix can be presented in the more compact way:

$$\mathcal{F}(\Theta) = \frac{\partial y(t, \Theta)}{\partial \Theta} \begin{bmatrix} \frac{1}{\sigma_{t_1}^2} & 0 & 0 \\ 0 & \ddots & 0 \\ 0 & 0 & \frac{1}{\sigma_{t_{n_t}}^2} \end{bmatrix} \frac{\partial y(t, \Theta)}{\partial \Theta^\top} \tag{33}$$

2.3.3. Cramer-Rao inequality

Let $\hat{\Theta}$ be an (absolutely) unbiased estimator Θ^*, i.e. such that it were possible to replicate the same experiment and estimate $\hat{\Theta}$ an infinite number of times, the mean of the estimates would coincide with the true value. Let Σ be the covariance matrix of this estimator. Since $\hat{\Theta}$ is unbiased, Σ can be written as

$$\Sigma = \underset{Y|\Theta^*}{\mathbb{E}} \left[\left(\hat{\Theta}(Y) - \Theta^* \right) \left(\hat{\Theta}(Y) - \Theta^* \right)^\top \right] \tag{34}$$

which quantifies how the estimates are spread around the true value Θ^*. One would like the estimates to be as concentrated as possible around this true value. An estimator $\hat{\Theta}_1$ with covariance matrix Σ_1 is said to be more efficient than an estimator $\hat{\Theta}_2$ with covariance matrix Σ_2 if $\Sigma_1 < \Sigma_2$, that is if $\Sigma_2 - \Sigma_1$ is positive-definite (i.e. if all the eigenvalues of $\Sigma_2 - \Sigma_1$ are strictly positive). Estimators with high efficiency are expected to have Σ as small as possible.

Under the hypotheses that:

- the set of all data vectors Y with $\pi_y(Y|\Theta) > 0$ does not depend on Θ

- $\frac{\partial \pi_y(Y|\Theta)}{\partial \Theta_i}$ $(i = 1, 2, ..., n_\Theta)$ is absolutely integrable

- $\mathbb{E}_{Y|\Theta} \left[\frac{\partial \ln(\pi_y(Y|\Theta))}{\partial \Theta} \frac{\partial \ln(\pi_y(Y|\Theta))}{\partial \Theta^\top} \right]$ exists and is invertible

The Cramer-Rao inequality provides that the covariance of any absolutely unbiased estimator satisfies

$$\Sigma \geq \mathcal{F}^{-1}(\Theta^*) \tag{35}$$

In other words, the precision to which we can estimate Θ is limited by the Fisher information of the likelihood function. Based on the Cramer-Rao inequality, the Fisher information matrix can used to calculate the covariance matrices associated with maximum-likelihood estimates.

2.3.4. Optimal experimental design

The optimal design of experiments (DOE) is a statistical concept that refers to the process of planning an experiment, which allow parameters to be estimated without bias and with minimum variance. Optimal design ensures that the experiment can provide the most informative data possible. This often involves balancing the study of main effects and interactions between factors. Moreover, by efficiently planning experiments, optimal design aims to reduce the overall resources required, such as time, materials, and manpower.

The methodology for data to estimate the parameters of a specific model is influenced by a series of qualitative decisions made throughout the experimental and modelling process, such as: a model structure, a location of sensors or an equipment. Once these choices have been made, the experimenter still has some freedom to specify the quantitative experimental conditions (such as temperature, pressure, sampling times, etc.). Experiment design aims to determine experimental conditions adapted to the final purpose of the modelling.

Let's consider that each scalar observation in a study can be expressed as $y(\xi_i)$, where the n_ξ-dimensional vector ξ_i representing the specific experimental conditions (such as the sampling time, operating conditions, etc.) under which the i'th observation is gathered. When collecting n_t such observations, the assembly of these ξ_i vectors forms the matrix $\Xi = (\xi_1, \xi_2, ..., \xi_{n_t})$, which combine all the experimental conditions that need optimization. In order to align the design of the experiment with practical realities, it's important to take into account various constraints, such as the total duration of the experiments, the maximum temperature of the inlet stream, or the minimum interval between sampling events. The set of all possible combinations for $\bar{\Xi}$ that adhere to these constraints is denoted as Ξ.

The formulation of a cost function j allows for the framing of optimal experiment design as a problem of constrained optimization. In this context, the optimal experiment, denoted as Ξ^*:

$$\Xi^* = \arg \underset{\Xi \in \bar{\Xi}}{\text{opt}} \, j(\Xi) \tag{36}$$

The cost function should describe the amount of information from an experiment. For that purpose it can be assumed a function κ can be related to the Fisher information obtained an arbitrary operating conditions.

$$j(\Xi) = \kappa \left[\mathcal{F}(\Theta, \Xi) \right] \tag{37}$$

A general class of DOE optimality criteria is given by

$$\kappa_k(\mathcal{F}(\Theta)) = \left[\frac{1}{n_\Theta} \text{trace} \left(Q\mathcal{F}^{-1}(\Theta, \Xi)Q^\top \right)^k \right]^{1/k} \quad \text{if } \det \mathcal{F} \neq 0$$
$$\kappa_k(\mathcal{F}(\Theta)) = \infty \quad \text{if } \det \mathcal{F} = 0 \tag{38}$$

where Q is a weighting matrix. The special case $k = 1$ corresponds to the L-optimality cost function,

$$j_L(\Xi) = \text{trace} \left[Q^\top Q\mathcal{F}^{-1}(\Theta, \Xi) \right] \tag{39}$$

and choosing $Q = \mathbf{I}_{n_\Theta}$ corresponds to the A-optimality cost function. An A-optimal experiment minimizes the sum of the squares of the lengths of the axes of asymptotic confidence ellipsoids. When Q diagonal, with $[Q]_{ii} = 1/\Theta_i$ this corresponds to C-optimality, which is associated with the relative precision of estimates. Selecting Q as a row vector results in C-optimality. Setting $Q = \mathbf{I}_{n_\Theta}$ and $k = \infty$ leads to E-optimality, where the design maximizes the smallest eigenvalues of the Fisher information matrix, thereby

minimizing the length of the largest axis of the asymptotic confidence ellipsoids. The most commonly used criterion is the D-optimality that involves $k = 0$, $Q = \mathbf{I}_{n_\Theta}$, requiring the minimization of $\det \mathcal{F}^{-1}(\Theta, \Xi)$, or, equivalently, maximization of

$$j_D(\Xi) = \det \mathcal{F}(\Theta, \Xi) \tag{40}$$

The D-optimality criterion originates from the geometric interpretation of the determinant. A two-dimensional matrix with real number entries can represent two linear maps: one mapping the standard basis vectors to the rows and the other to the columns. In both cases, the images of the basis vectors form a parallelogram that represents the image of the unit square under the mapping. The absolute value of the determinant is the area of this parallelogram, reflecting the scale factor by which the matrix transforms areas. The signed value of the determinant indicates the oriented area of the parallelogram, which is negative when the angle from the first to the second defining vector is clockwise. In the multi-dimensional case, the matrix maps the n-cube to an n-dimensional parallelotope. The determinant provides the signed n-dimensional volume of this parallelotope, describing the volume scaling factor of the linear transformation produced by the matrix. Based on this geometric interpretation, a D-optimal experiment minimizes the volume of the asymptotic confidence ellipsoids for the parameters. Figure 5 illustrates the graphical representation of different optimality conditions.
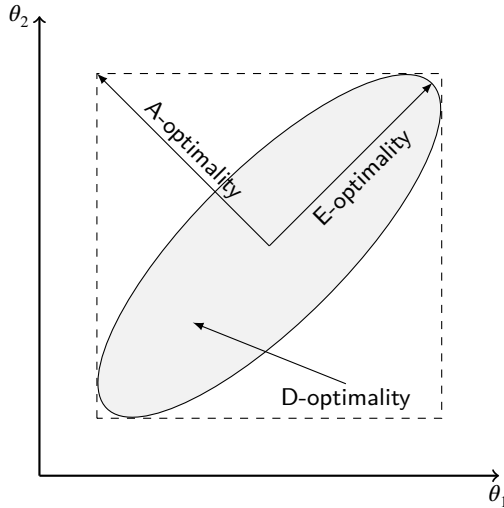

Figure 5: Graphical representation of score functions

2.3.5. Problem formulation

Details on the process model can be found in [article 1]. The model's empirical correlations are derived based on laboratory experiments conducted under various constant operating conditions: $30 - 40°C$, $100 - 200$ bar, and $3.33 - 6.67 \cdot 10^{-5}$ kg/s. This study employs a model-based design of experiments technique to design an experiment with dynamically changing conditions to improve the precision of

the correlation for D_i. The decision variables are adjusted every 10 minutes and are kept constant within each interval (piecewise constant controls). These controls have lower and upper bounds that match the validated range of the process model detailed in [article 1]. The sampling time is set to 5 minutes, and the total extraction time is 300 minutes. The standard deviation σ^2 was estimated to be 0.12. The analysed correlations consist of two independent variables: Reynolds number and mass flow rate. The Reynolds number is a function of fluid thermodynamic properties and velocity, and the fluid density can be affected by temperature or pressure changes. In this work, both cases are solved and compared.

In the first case, the decision variables are the inlet temperature (T^{in}) and mass flow rate (F). Throughout the experiment, the pressure is assumed to remain constant at 150 bar (the middle of the validated range). The initial state is considered isothermal, so $T^0 = T^{in}(t = 0)$. The problem formulation for Case 1 is given by Equation 41.

$$
\begin{aligned}
\Xi^* \quad &= \arg \min_{T^{in}, F \in \Xi} \int_{t_0}^{t_f} -\ln j_D(\Xi, \dot{x}) dt \\
\text{subject to} \quad &\dot{x} = G(x, t, \Theta; \Xi) \\
&t_0 = 0 \quad \min \\
&t_f = 300 \text{ min} \\
&T^0 = T^{in}(t = 0) \\
&P(t) = 150 \text{ bar} \\
&30°C \leq T^{in}(t) \leq 40°C \\
&3.33 \cdot 10^{-5} \leq F(t) \leq 6.67 \cdot 10^{-5}
\end{aligned} \tag{41}
$$

In the second case, the pressure and mass flow rate are treated as decision variables, while the inlet temperature is kept constant at $35°C$. Similar to the first case, the extractor is assumed to be isothermal at the beginning of the operation. Unlike the previous case, changes in pressure affect the temperature inside the extractor. Any temperature deviation caused by pressure changes will eventually be mitigated by the inflow of fresh fluid at the constant temperature of $35°C$. The problem formulation for Case 2 is given by Equation 42.

$$
\begin{aligned}
\Xi^* \quad &= \arg \min_{P, F \in \Xi} \int_{t_0}^{t_f} -\ln j_D(\Xi, \dot{x}) dt \\
\text{subject to} \quad &\dot{x} = G(x, t, \Theta; \Xi) \\
&t_0 = 0 \quad \min \\
&t_f = 300 \text{ min} \\
&T^0 = T^{in}(t) = 35°C \\
&100°C \leq P(t) \leq 200°C \\
&3.33 \cdot 10^{-5} \leq F(t) \leq 6.67 \cdot 10^{-5}
\end{aligned} \tag{42}
$$

3. Results

To identify the global solution of Equations 41, the optimization problem is solved multiple times, each starting from a random initial solution. Figure 6 compares the initial and final values of the cost function across multiple optimization runs. The shaded area spans from the smallest to the third smallest final values of the objective function. The black curves on the left and below the scatter plot represent the distributions of the initial and final cost function values,

respectively. From Figure 6, it can be observed that multiple local solutions exist for Case 1. The solution with the lowest cost function value is considered the global solution.
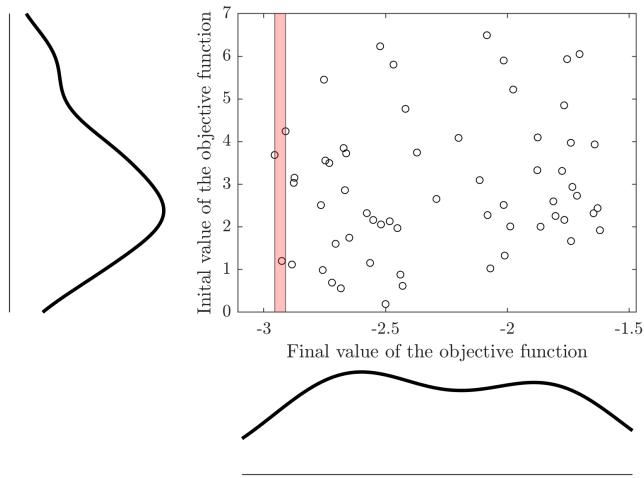
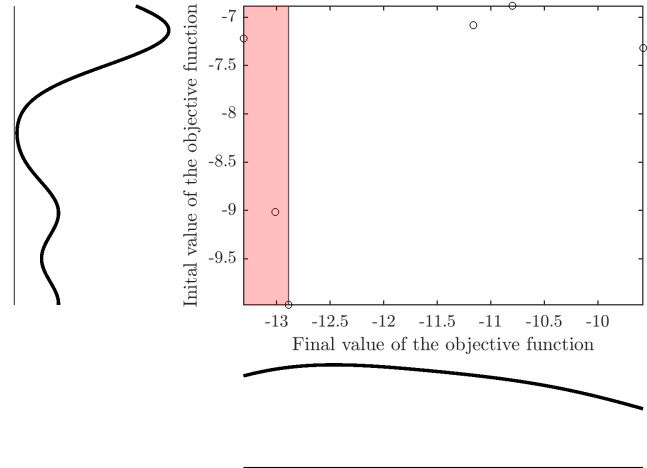**Figure 6:** Initial vs final values of the cost function

The optimal profiles of inlet temperature and mass flow rate are presented in Figure 7. One of the independent parameters in the analysed correlation is the mass flow rate, which is directly modified several times during the experiment. The second independent parameter is the Reynolds number, which can be affected by changes in the thermodynamic properties of the fluid. The thermal properties of CO_2 between 30°C and 40°C, assuming a constant pressure of 150 bar, vary only slightly. For instance, the dynamic viscosity changes from 67 to 80×10^{-6} Pa·s. The obtained profile of the inlet temperature shows minimal variation, suggesting a limited influence of inlet temperature on the extraction yield. Given the narrow operational window for inlet temperature at constant pressure, the mass flow rate becomes the primary variable to control.
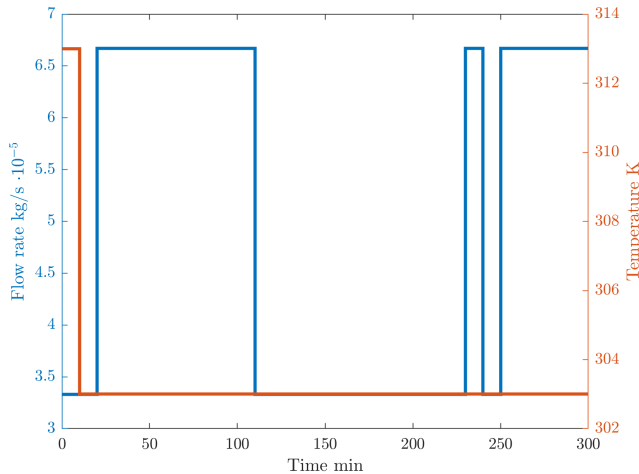
**Figure 7:** Optimal temperature and mass flow rate profiles

Similar to Case 1, Case 2 is solved multiple times starting from random initial solutions to identify the global

solution. Figure 8 summarizes the changes in the objective function values across all optimization runs. It is evident that both the initial and final values of the cost function are significantly lower than any values obtained in Case 1. In Case 2, the wider operating range leads to more significant changes in the physical properties of CO_2 compared to Case 1. For example, the kinematic viscosity of CO_2 ranges from $48 \cdot 10^{-6}$ (at 40°C and 100 bar) to $90 \cdot 10^{-6}$ Pa·s (at 30°C and 200 bar). The greater variability in pressure induces a more complex system response, including temperature variations, resulting in lower values of the objective function compared to Case 1.

Figure 8: Initial vs final values of the cost function

The optimal profiles of pressure and mass flow rate are presented on Figure 9. Similarly to case 1, only few changes in the mass flow rate are observed in the plot. In contrary to the inlet temperature, the pressure changes are frequently applied in the case 2.
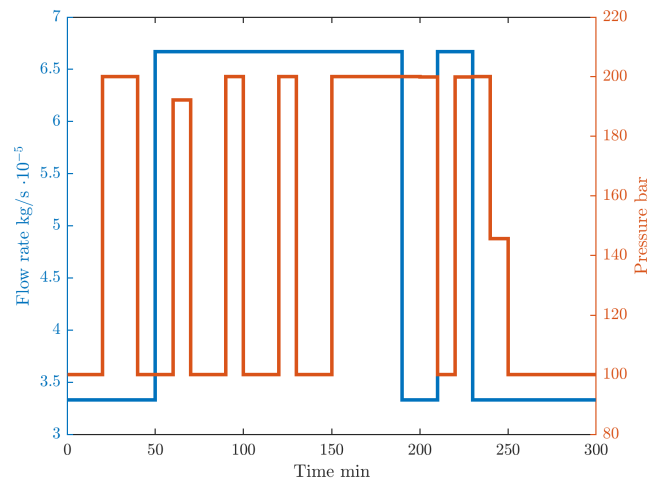
Figure 9: Optimal pressure and mass flow rate profiles

4. Conclusions

References

[1] O. Singh, Z. Khanam, N. Misraand, and M.K. Srivastava. Chamomile (matricaria chamomilla l.): An overview. Pharmacognosy Reviews, 5 (9):82, 2011. ISSN 0973-7847. doi: 10.4103/0973-7847.79103.

[2] J. Srivastava. Extraction, characterization, stability and biological activity of flavonoids isolated from chamomile flowers. Molecular and Cellular Pharmacology, 1(3):138–147, August 2009. ISSN 1938-1247. doi: 10.4255/mcpharmacol.09.18.

[3] A. Orav, A. Raal, and E. Arak. Content and composition of the essential oil ofchamomilla recutita(l.) rauschert from some european countries. Natural Product Research, 24(1):48–55, January 2010. ISSN 1478-6427. doi: 10.1080/14786410802560690.

[4] E. Reverchon, G. Donsi, and L.S. Osseo. Modeling of supercritical fluid extraction from herbaceous matrices. Industrial & Engineering Chemistry Research, 32(11):2721–2726, nov 1993. doi: 10.1021/ie00023a039.

[5] H. Sovova. Rate of the vegetable oil extraction with supercritical co2. modelling of extraction curves. Chemical Engineering Science, 49 (3):409–414, 1994. doi: 10.1016/0009-2509(94)87012-8.

[6] E. Reverchon. Mathematical modeling of supercritical extraction of sage oil. AIChE Journal, 42(6):1765–1771, June 1996. ISSN 1547-5905. doi: 10.1002/aic.690420627.

[7] R.A Fisher. The Design of Experiments. Olivier & Boyed, 1935.

[8] N.F. Ramandi, N.M. Najafi, F. Raofie, and E. Ghasemi. Central composite design for the optimization of supercritical carbon dioxide fluid extraction of fatty acids fromborago officinalisl. flower. Journal of Food Science, 76(9), October 2011. ISSN 1750-3841. doi: 10.1111/j.1750-3841.2011.02394.x.

[9] G. Caldera, Y. Figueroa, M. Vargas, and D.T. Santos. Optimization of supercritical fluid extraction of antioxidant compounds from venezuelan rosemary leaves. International Journal of Food Engineering, 8(4), October 2012. ISSN 1556-3758. doi: 10.1515/1556-3758.1953.

[10] S.H. Chung, D.L. Ma, and R.D. Braatz. Optimal model-based experimental design in batch crystallization. Chemometrics and Intelligent Laboratory Systems, 50(1):83–90, January 2000. ISSN 0169-7439. doi: 10.1016/s0169-7439(99)00049-0.

[11] B. Duarte, A. Atkinson, J. Granjo, and N. Oliveira. Calculating d-optimal designs for compartmental models with a michaelismenten elimination rate. Journal of Process Control, 83:88–101, November 2019. ISSN 0959-1524. doi: 10.1016/j.jprocont.2019.09.001.

[12] J. D. Jr Anderson. Computational fluid dynamics the basic with applications. McGraw-Hill, 1995. ISBN 9780071132107.

[13] J. D. Jr Anderson. Fundamentals of Aerodynamics. McGraw-Hill Education, 2023. ISBN 9781264151929.

[14] N. R. Bulley, M. Fattori, A. Meisen, and L. Moyls. Supercritical fluid extraction of vegetable oil seeds. Journal of the American Oil Chemists' Society, 61(8):1362–1365, aug 1984. doi: 10.1007/bf02542243.

[15] M. Spiro and M. Kandiah. Extraction of ginger rhizome: partition constants and other equilibrium properties in organic solvents and in supercritical carbon dioxide. International Journal of Food Science & Technology, 25(5):566–575, jun 2007. doi: 10.1111/j.1365-2621.1990.tb01116.x.

[16] H. Sovova. Broken-and-intact cell model for supercritical fluid extraction: Its origin and limits. The Journal of Supercritical Fluids, 129:3–8, nov 2017. doi: 10.1016/j.supflu.2017.02.014.

[17] M. Goto, B.C. Roy, and T. Hirose. Shrinking-core leaching model for supercritical-fluid extraction. The Journal of Supercritical Fluids, 9 (2):128–133, jun 1996. doi: 10.1016/s0896-8446(96)90009-1.

[18] J. Gmehling, M. Kleiber, B. Kolbe, and J. Rarey. Chemical Thermodynamics for Process Simulation. Wiley, mar 2019. doi: 10.1002/9783527809479.

[19] H. Sovova, R. Komers, J. Kucuera, and J. Jezu. Supercritical carbon dioxide extraction of caraway essential oil. Chemical Engineering Science, 49(15), 1994. doi: 10.1016/0009-2509(94)e0058-x.

[20] E. Walter and L. Pronzato. Identification of parametric models from experimental data. Communications and control engineering. Springer, London, 2010. ISBN 9781849969963.